

THE ENHANCED INJECTION AND MIXING PROJECT AT NASA LANGLEY

K. F. Cabell, T. G. Drozda, E. L. Axdahl and P. M. Danehy
NASA Langley Research Center
Hampton, Virginia

ABSTRACT

An overview of a research project aimed at enhancing fuel injection and mixing for scramjet engines at flight Mach numbers greater than 8 is presented. The specific objectives of this project are to increase knowledge and understanding of the fundamental physics governing scramjet fuel-air mixing, to develop strategies for improving injector performance and to develop functional relationships between mixing efficiency, losses due to mixing (such as total pressure loss, drag) and combustor/mixing length. The research approach consists of a closely coupled experimental and computational effort with experiments intended for exploring injection concepts and for anchoring computational fluid dynamics (CFD) simulations. The experiments are being conducted in the NASA Langley Arc-Heated Scramjet Test Facility and consist of helium injection into a Mach 6 air stream. Measurements include in-stream helium mole fraction, pitot pressure, and total temperature as well as wall pressures and temperatures. Additionally, nitric oxide planar laser-induced fluorescence (NO PLIF) imaging will be used for flow visualization of the fuel plume. The numerical simulations, performed with the VULCAN CFD code, provide flowfield details unobtainable from the experiment. The current paper describes the experimental apparatus and diagnostic systems that have been developed and/or tested in preparation for the mixing tests and discusses numerical simulations performed to reduce the risk associated with the experimental design.

INTRODUCTION

Many of the challenges associated with high-speed, air-breathing propulsion powered flight have been previously studied at flight Mach numbers of 10 and below, culminating in successful flights of vehicles such as the X-43A and X-51. Extending scramjet operation to higher Mach numbers offers the potential for increased efficiency in delivering payloads to space. By increasing the staging Mach number of a two-stage-to-orbit vehicle, less on-board oxygen would be required, resulting in a larger fraction of the take-off weight available for payload or added structure/systems for increased ruggedness and flexibility.¹ However, with increasing flight Mach number, effective injection and mixing of fuel into the extremely high velocity airflow without introducing excessive drag becomes a key challenge, especially because rapid mixing is needed to enable a shorter combustor length thereby reducing vehicle weight and thermal loads. The Enhanced Injection and Mixing (EIM) project currently underway at the NASA Langley Research Center is aimed at addressing the challenge of achieving rapid mixing while minimizing losses for flows with very high velocities characteristic of high Mach number flight. The project is a coupled experimental and computational research effort to study the fundamental physics of injection and

mixing relevant to scramjets at flight Mach numbers between 8 and 20 with an ultimate goal of improving scramjet performance and design capability.

Specific objectives of the current project are enumerated below. The payoff and impact of meeting these objectives is higher performance injectors for high Mach flight and performance-loss relationships that can be used for optimization of scramjet flowpaths and flight vehicles.

1. To increase knowledge and understanding of the fundamental physics governing fuel-air mixing relevant to the hypervelocity flight regime.
2. To develop strategies for improving injector performance (increased mixing efficiency, reduced losses/drag).
3. To develop the functional relationships between mixing efficiency, losses (i.e., total pressure loss, drag) and flowpath geometry (i.e., combustor length, injector spacing).

The NASA Langley integrated experimental, advanced diagnostic, and computational capabilities will be applied toward meeting these objectives. These include the design and execution of wind-tunnel tests simulating relevant flight conditions, nonintrusive laser-based diagnostics for visualization of the fuel plume, and state-of-the-art computational tools for simulating high Mach, multispecies flow.

The experiments, conducted in the NASA Langley Arc-Heated Scramjet Test Facility (AHSTF),²⁻⁴ include tests of various fuel injection devices mounted on an open flat plate located downstream of a Mach 6 facility nozzle that simulates a combustor entrance Mach number for flight at Mach 14 to 16. The current experiments focus on nonreacting mixing processes by utilizing an inert gas as a fuel simulant. Helium was chosen because it has a molecular weight close to that of hydrogen gas, which is an expected fuel for the flight range of interest. Nonreacting studies are justified because, with increasing flight Mach number, the combustion heat release is a smaller fraction of the total enthalpy, yielding less pressure rise and therefore, a smaller impact on the flow structure in the combustor. Furthermore, the effect of combustion has been shown to reduce the rate of growth of the mixing layer,¹ but this effect also diminishes with increasing flight Mach number, again because the heat release is a smaller fraction of the total enthalpy. A consequence of neglecting the effect of heat release is that the total enthalpy of the experiment can be reduced to limit the thermal stresses on the experimental hardware. In the current experiments, the maximum total enthalpy has been limited to a value that corresponds to about Mach 4 flight conditions.

Two complementary diagnostic techniques are being employed to characterize the fuel plume. The first leverages the NASA Langley advanced laser-based diagnostic capability and will use nitric-oxide planar laser induced fluorescence (NO PLIF) to visualize the fuel plume and the second technique is an in-stream probe based gas sampling and analysis system (GSAS) to directly measure helium mole fraction distributions. Although the underlying gas sampling and analysis technique is straightforward, the GSAS requirements, derived from diagnostic uncertainty analysis and overall mixing research objectives, led to a relatively complex forty-probe system and to an extended test duration requirement.

Computational fluid dynamics (CFD) is used to provide details of the flowfield not available from the experiment and provide insight into the flow features that control mixing. CFD simulations are also needed to compute performance metrics such as mixing efficiency, total pressure recovery, and stream thrust potential. All simulations are being performed with the VULCAN CFD code⁵ and consist primarily of Reynolds-averaged simulations (RAS), which utilize conventional and well-understood turbulence models and are applied following experience-based best practices for the problems of interest. The most promising injector configurations will be simulated via large-eddy simulations (LES), which, although computationally more expensive than Reynolds averaged simulations, provide significantly more details of the flow. Additionally, the CFD simulations provided pretest predictions that have significantly aided the design of the experiment.

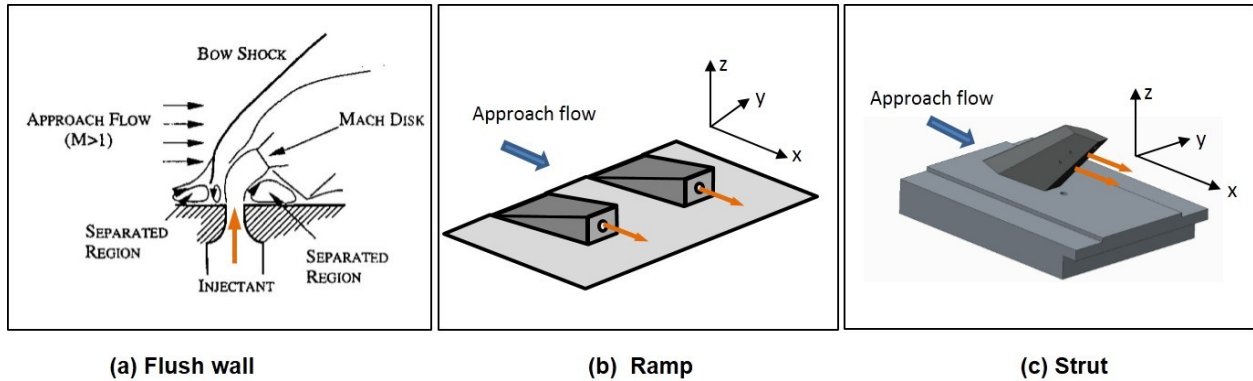


Figure 1: State of the art injection types: (a) Flush wall (side view of normal injection with flow schematic)⁶ and isometric views of generic (b) Ramp and (c) Strut injector geometries.

The current state of the art in fuel injection methods can be divided into three basic types: flush wall injection (perpendicular and angled), ramp injection and strut injection. Generic illustrations of each are shown in Figure 1. The flush-wall type injects directly from ports on the surface of the combustor wall. The separated regions directly upstream and downstream of the fuel jet act as flame holders.¹ Ramps protrude partly into the flow and provide mixing enhancement by producing streamwise vorticity as the flow rolls off the top of the ramp. Struts protrude into the core of the flow to improve penetration compared to flush-wall and ramp injectors, but at the cost of additional shock losses and drag. Each of these injection types is being considered in the present effort, however, a strut injector employing near parallel injection has been chosen as a baseline for the initial experiments and computational simulations. This choice is motivated by the fact that in high Mach number flight, it is increasingly difficult to penetrate the core flow of the flowpath, therefore, a fuel placement device is required. Furthermore, the axial momentum provided by parallel injection is expected to offset some of the drag generated by the injector body; this also becomes more important in high Mach number flight where the heat release due to combustion is an increasingly smaller fraction of the total enthalpy and therefore, provides a smaller contribution to the momentum gain realized in the nozzle expansion process.

The remainder of this paper provides further overview of the experimental considerations, a description of the test apparatus and in-stream gas sampling system developed specifically for this project, a description of the flow visualizations via the NO PLIF technique, and it highlights pretest CFD analysis that aided the design of the experiment. The paper concludes with a summary and discussion of future work.

EXPERIMENT DESCRIPTION

OVERVIEW

The combustor entrance Mach number and Reynolds number are two of several key parameters to match for mixing simulations. The flight Mach number range of interest is Mach 8 to 20, which corresponds to combustor entrance Mach numbers between approximately 3 and 7 and unit Reynolds numbers on the order of 5×10^6 per foot. The exact values of Mach and Reynolds number are a function of the specific inlet design, which is beyond the scope of this paper. Herein, a flight vehicle traveling along a 1500 psf dynamic pressure trajectory and experiencing 5% entropy gain and 1% total enthalpy loss during forebody and inlet compression is assumed. With these assumptions, the AHSTF Mach 6 facility nozzle simulates the combustor entrance Mach number for flight at Mach 14 to 16. The maximum total

Table 1: Test Conditions

| Stagnation Conditions in Facility Plenum | | |
|--|-----------------|-----------------|
| Property | Min-temperature | Max-temperature |
| Total pressure (psia) | 625 | 625 |
| Total temperature (R) | 1310 | 1760 |
| Facility Nozzle Exit Conditions | | |
| Property | Min-temperature | Max-temperature |
| Mach | 6.48 | 6.40 |
| Static pressure (psia) | 0.25 | 0.25 |
| Static temperature (R) | 145 | 200 |
| Velocity (ft/s) | 3787 | 4435 |
| Reynolds number (1/ft) | 5e+06 | 3e+06 |

temperature was limited to 1760°R to allow for uncooled test hardware, and the minimum total temperature was limited to 1310°R to prevent oxygen condensation as the nozzle air flow expands. The stagnation pressure is set at the maximum capability of the facility, which is 625 psia. Parameters of interest for the minimum and maximum temperature conditions are provided in Table 1. The facility nozzle exit conditions shown were estimated assuming one-dimensional isentropic flow with variable specific heats. The facility nozzle exit Mach number is higher than 6 because the facility nozzle was designed⁷ to yield a Mach 6 flow at a Mach 7 total temperature (3760°R) and the lower range of temperatures for the present tests result in a higher calculated Mach number due to the higher ratio of specific heats. Furthermore, vibrational non-equilibrium effects, known to exist under the AHSTF's typical Mach 6 to 8 enthalpy operation, have been assessed and were found to be minimal under the conditions planned for this test (as will be shown later).

A side view of the test apparatus, which has been designed and fabricated, is shown in Figure 2. The fuel injectors will be mounted on an open test bed plate, which is positioned horizontally inside the 4-foot diameter test cabin, immediately downstream of the 10-in. x 10-in. facility nozzle exit. An open plate design was chosen instead of a closed duct to facilitate optical access; the lack of combustor walls was deemed acceptable due to the fundamental nature of this study. The test bed plate is 29 inches long by 32 inches wide and accommodates the installation of interchangeable injector blocks, which are 4 inches long and axially centered 7 inches downstream of the plate leading edge. The test bed plate has been installed, as shown in Figure 3, with a flush wall injector for preliminary testing of the gas sampling system (described later). The strut injector, selected as a baseline for initial mixing tests and computational simulations is a modification of that studied by Baurle et al.⁸ at Mach 4.5 cold flow conditions. The modification included an addition of a fourth fuel port to account for the removal of adjacent interdigitated injectors present in the original configuration. The EIM project plans include testing an array of five struts, as shown in the CAD image of Figure 4(a). The injector blocks are fabricated at an on-site facility using the the Selective Laser Melting (SLM) manufacturing technique. This rapid fabrication process is expected to shorten turnaround time to test new injectors and therefore, enable rapid screening of injection concepts. The on-site facility has demonstrated this technique on struts of similar design. An example is shown in the photograph of Figure 4(b).

As explained earlier, helium has been selected as the fuel simulant. The mass flow rate of helium is set equal to that for hydrogen at a fuel equivalence ratio of 1.0. In other words, the "fuel"-air mass ratio is equal to the stoichiometric fuel-air mass ratio for hydrogen. However, the air mass flow rate must be specified. The air mass flow is determined by assigning a cross-sectional area of the flow that the injector is intended to fuel (i.e., assuming it were inside a closed duct) and estimating the approaching air mass flux (i.e., the nozzle centerline exit mass flux, as determined from CFD) over that area.

Standard facility measurements include the facility air flow rate, the stagnation pressure in the plenum upstream of the facility nozzle, nozzle wall pressures and test cabin wall pressures. The air mass flow

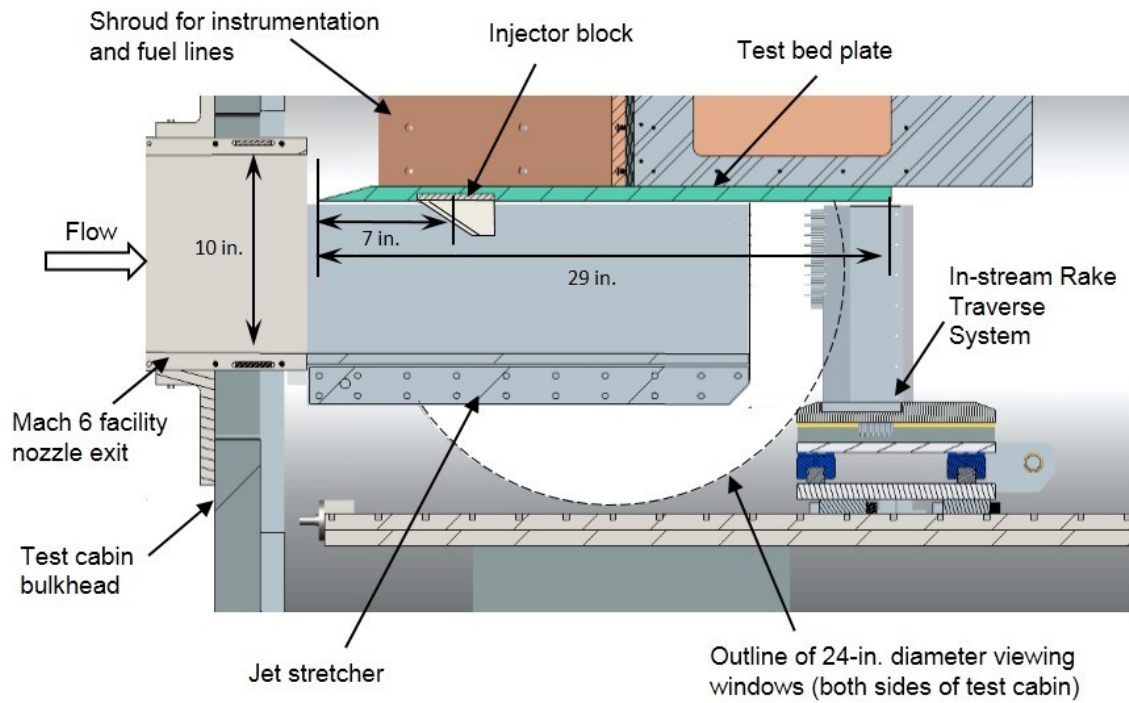


Figure 2: Side view of test apparatus installed in AHSTF.

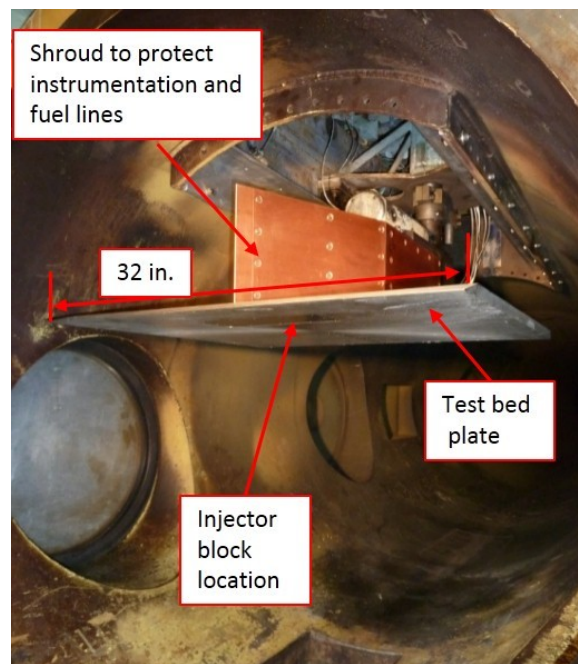


Figure 3: Test bed plate installed in AHSTF test cabin; view looking downstream with test cabin bulkhead and facility nozzle removed.

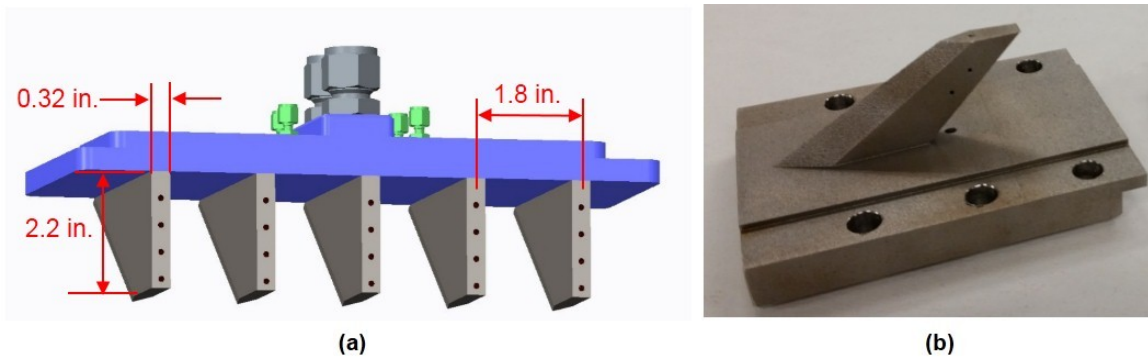


Figure 4: (a) CAD image of baseline strut injector block and (b) photograph of a single strut manufactured by SLM.

rate, plenum stagnation pressure and facility nozzle throat area are used to derive the stagnation enthalpy from a sonic throat method.⁹ The flow rate of helium delivered to the injector block will be derived from pressure and temperature measurements upstream of a calibrated sonic venturi. The suite of mixing region instrumentation includes test bed plate surface pressures and temperatures as well as in-stream measurements of pitot pressure, total temperature and helium mole fraction. The mole fraction distribution will be used to calibrate the turbulent Schmidt number used in the CFD and all other mixing region measurements will be used to validate the CFD solution. The in-stream measurements can be obtained within a measurement volume adjacent to the test bed plate, having a 5-in. x 5-in. cross-section and spanning the length of the test bed plate. The helium mole fraction is measured by a gas sampling and analysis system to be described in the next section. All of the in-stream measurements are obtained from probes mounted on an automated traversing rake system shown in Figure 2. In a single test, a system of three vertically oriented rakes, shown in Figure 5, traverse laterally across a survey plane perpendicular to the free stream flow direction. The rakes and traverse system have been designed and fabricated; integration into the facility is underway. The axial position of the survey plane can be changed between tests and is infinitely adjustable within a distance of 30 inches downstream of the facility nozzle exit plane (20 inches downstream of the fuel injector block trailing edge). Because of conditions where the facility nozzle may be under- or over-expanded, jet stretchers (extensions of the nozzle bottom wall and sidewalls) are necessary to prevent expansion or compression waves from interfering with the flow upstream of the survey plane. Calculations were performed to determine that a jet stretcher exit plane no more than five inches upstream of a given survey plane accomplishes this objective, leaving a 5-in. long unobstructed region for optical access. To accommodate the full length of the measurement volume, four sets of jet stretchers (of varying length: 10, 15, 20 and 25 inches) have been designed and fabricated.

The survey plane size of 5-in. x 5-in. was chosen to be well within the uniform core of the facility nozzle exit flow (to be shown in a later section) and the gas sample measurement spacing of every 0.125 inches was chosen based on considerations of practical probe size and probe interference. This survey plane size and measurement spacing led to a requirement of 40 probes. The probes are distributed among two rakes of 20 probes each, as shown in Figure 5. Additionally, the estimated gas sampling time per probe led to a test duration requirement estimate of 5 to 6 minutes. Because the facility had never been operated for durations greater than one minute, a series of longer duration tests were conducted, as risk reduction, in order to discover any unforeseen limitations to run duration (such as a power supply limit, hardware thermal limits, vacuum system limit). The test duration was initially set at 30 seconds and was increased by 30 seconds with successive tests. The maximum test duration achieved was 5 minutes and 23 seconds and both facility hardware temperatures and test cell pressures remained well within acceptable limits for this test duration. However, after a 3.5 minute test, it was discovered that unacceptably large amounts of copper were being released into the air from the arc-heater

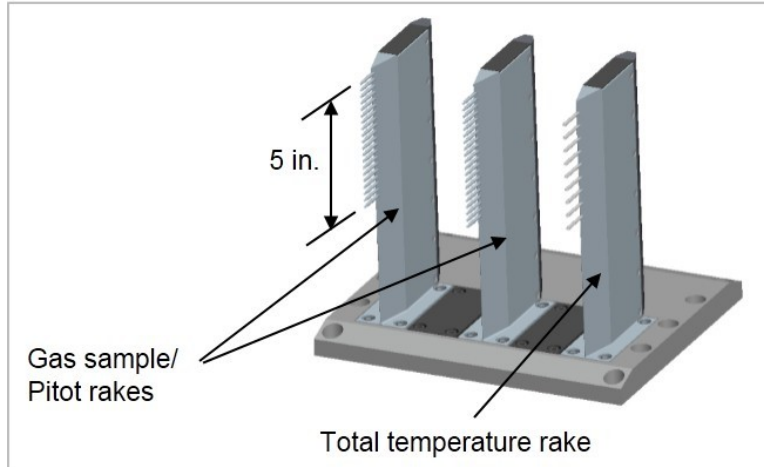


Figure 5: In-stream traversing rakes.

electrodes. The copper pieces became lodged in the 0.10-in. high facility nozzle throat as evidenced during the test by a sudden increase in plenum pressure and subsequently confirmed by visual inspection of the heater and nozzle throat. The copper was removed from the throat and additional longer tests were conducted, however, the problem occurred more frequently and after a shorter period of continuous arc operation. It was concluded that continuous arc operation for a duration greater than 3.5 minutes results in electrode wall temperatures reaching the melting point where the arc attaches to the electrodes. Consequently, the copper melts and is released into the air. It likely occurs after a shorter test time for subsequent tests because of the loss of copper/thermal mass at the attachment point. Therefore, the mixing tests will be limited to less than 3.5 minutes, and either the measurement density or the width of the survey plane for a given test will be reduced.

GAS SAMPLING AND ANALYSIS SYSTEM

The gas sampling and analysis system (GSAS) consists of forty gas sample probes connected to the necessary tubing and valves to direct the sampled gas over a constant temperature anemometer (CTA) placed upstream of a choked orifice. The technique has been developed, described and applied by many¹⁰⁻¹³ to make concentration measurements in binary gas mixtures. In the present application, the binary mixture is helium and air. With the choked orifice downstream of the CTA, the velocity at the CTA is a function only of the gas composition and temperature at the CTA. The CTA voltage is then a function of the gas composition, pressure and temperature at the CTA. As in the system described by Cutler and Johnson,¹² the calibration process is simplified by maintaining a constant gas temperature and pressure at the CTA, which results in the CTA voltage being a function of only the gas composition and therefore, helium mole fraction. A maximum measurement uncertainty of ± 0.01 mole fraction of helium was set as a goal based on what was deemed necessary to identify the fuel plume boundary.

For sampling in supersonic flows, the sample probe must be designed to be shock swallowing because of the possibility of light gas separation caused by a normal shock in front of the probe.¹⁴ The sample probe design is shown in Figure 6(a), and a photograph of two probes installed on a rake is shown in Figure 6(b). The probe has a standing shock located inside the diverging probe tip as long as the back pressure is maintained low enough. Between each probe and the CTA, there is approximately 10 feet of "transfer tube" necessary to route the gas outside the AHSTF test cabin to the CTA. A simplified two-probe GSAS schematic is shown in Figure 7. For each probe, there are two sample valves that direct the flow either to the CTA or to a vacuum source for evacuation prior to sampling; these are

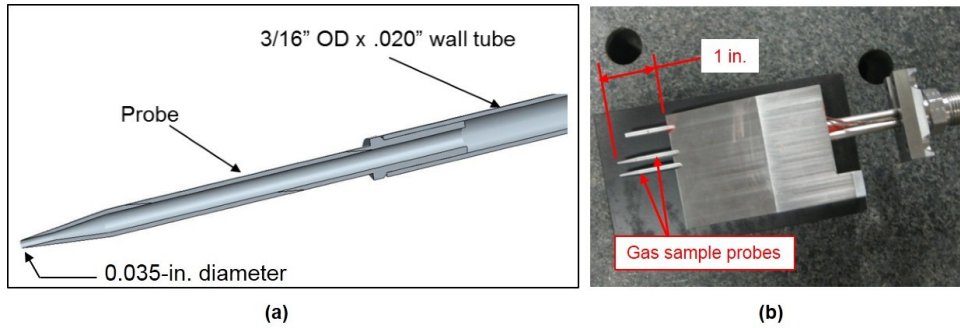


Figure 6: (a) Gas sample probe details and (b) Two gas sample probes mounted on a rake.

denoted as “SV” or “PV”, respectively, in the schematic. Pre-evacuation shortens the time needed for a fresh sample to arrive at the CTA because a majority of the transfer tube is filled with sample gas. Note that by closing both sample valves (SV and PV) for a given probe, a pitot pressure measurement is obtained via a transducer located just upstream of the valves. The sample gas is thermally conditioned to 68°F by submersion of the tube in a temperature-controlled water bath. Just upstream of the CTA, a majority of the gas captured by the probe is vented to a large reservoir maintained at constant pressure; the intent of this is to maintain the gas at the CTA equal to that same constant pressure. The system was designed for the range of expected conditions in the mixing region as provided by the pretest CFD of the baseline strut injector (to be shown in a later section). Very low predicted pitot pressures in the fuel plume drove the transfer tube back pressure requirement (and therefore, the CTA pressure and the reservoir pressure) to be 0.50 psia. This pressure is maintained by a vacuum regulator and a large vacuum source connected to the outlet of the reservoir. Finally, a calibration system, consisting of helium and air supplies and flow controllers for each, allows a gas of known helium mole fraction to be delivered to the CTA for calibration. In addition to CTA voltage, the pressure and temperature of the gas at the CTA are measured during a test to verify that they are equal to their values during calibration. The pressure downstream of the choked orifice is also measured during both calibration and test, to verify choked flow conditions. For the purpose of further discussion, the pressure and temperature of the gas at the CTA are hereafter referred to as the “CTA pressure” and the “CTA temperature”, respectively (where “CTA temperature” is not to be confused with the temperature of the anemometer itself).

Compared to the simplified system depicted in Figure 7, the full forty-probe GSAS consists of eighty sample valves that distribute the forty samples to either one of four CTA’s or to the vacuum source for pre-evacuation. A control system, which is integrated with the rake traverse control system, opens and closes the necessary valves to sample all forty probes at each rake position. The full GSAS has been designed and fabricated (see photograph shown in Figure 8) and the control system assembly is underway. However, because of the relative complexity of the system and lack of in-house experience with such a system, a simplified demonstration version of the full system, schematically equivalent to the system shown in Figure 7, was built and tested first. Example calibrations from this “Demo” system are shown in Figure 9. Figure 9(a) shows calibrations at a pressure of 0.5 psia and two different temperatures and Figure 9(b) shows calibrations at a temperature of 68°F and three different pressures. The CTA sensitivity (change in voltage per change in mole fraction) will allow a measurement resolution well below the ± 0.01 mole fraction uncertainty goal; however, the actual measurement uncertainty (due to the uncertainty in the measurements of calibration gas flow rates and CTA pressure and temperature) is yet to be determined. Note the sensitivities to pressure and temperature are significant. For example, from Figure 9(b), it can be seen that at a helium mole fraction of 0.50, if the actual CTA pressure is 0.4 psia, the application of a calibration conducted at 0.5 psia would result in a deduced mole fraction of 0.45. This underscores the need for accurate knowledge of the CTA pressure and temperature and the need to calibrate as a function of pressure and temperature if, during a test, they cannot be maintained constant and equal to their respective calibration values.

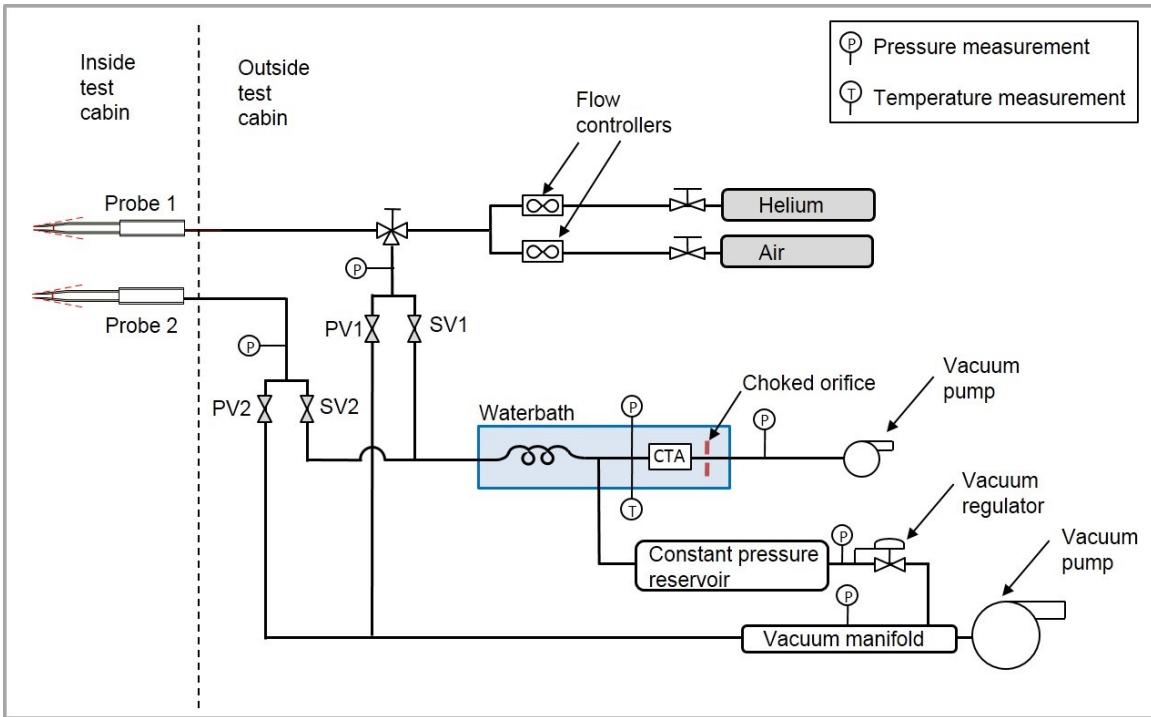


Figure 7: Simplified gas sampling and analysis system (GSAS) schematic.

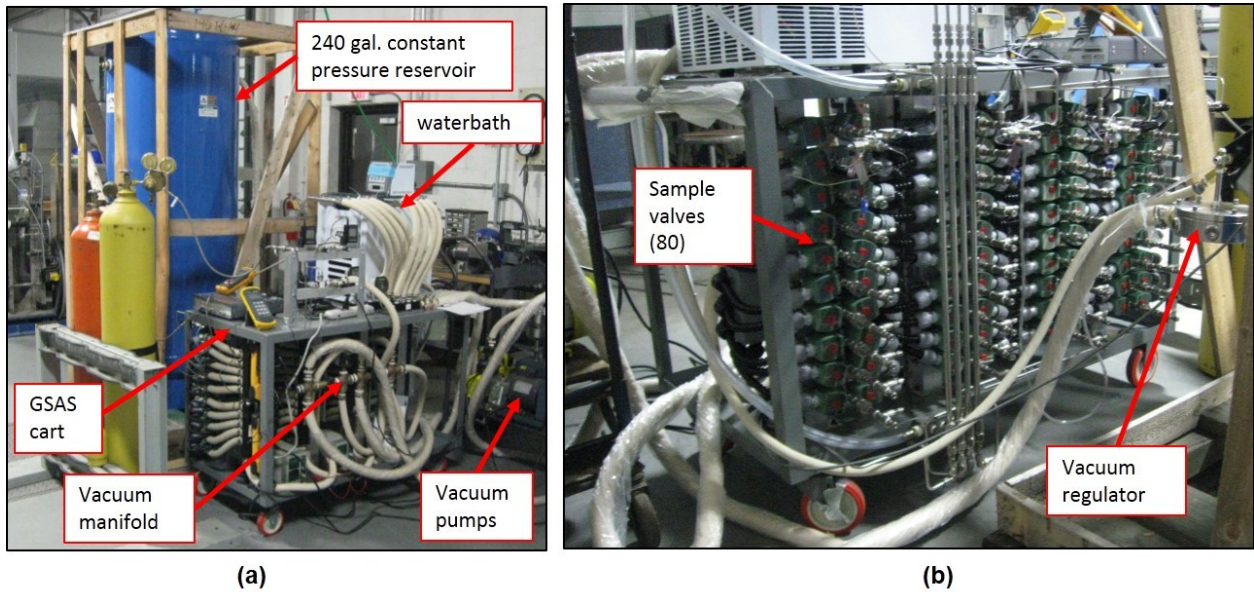


Figure 8: Photographs of the full GSAS showing (a) front of GSAS cart and (b) 80 sample valves mounted on back side of cart.

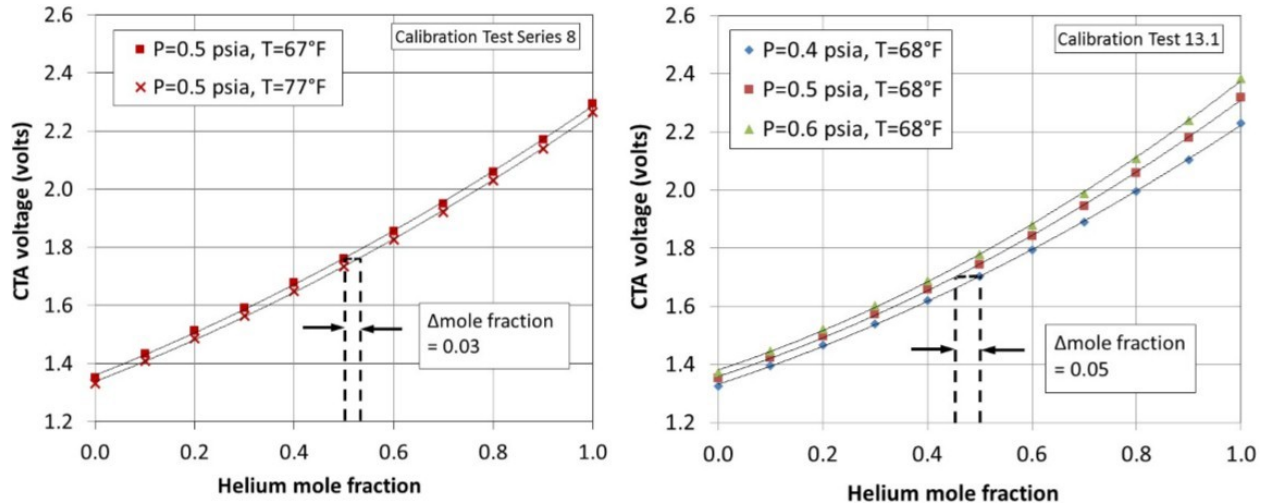


Figure 9: CTA calibrations obtained with the Demo GSAS.

Wind tunnel tests of the Demo GSAS with a two-probe rake (shown in Figure 6(b)) installed on the test bed plate downstream of a flush wall injector were conducted. A schlieren system was set up to confirm expected wave structures (bow shocks from the test bed plate leading edge and the fuel plume) and to visualize the shocks around the gas sample probes to verify shock swallowing. Gas samples were successfully collected under tare and fuel-on conditions, although not over the full range of target fuel injector pressures desired to vary the penetration and thus, mole fraction at the fixed probe positions. Results are not shown here for brevity, however, the most important findings are as follows: 1) the time response of the CTA voltage, pressure and temperature when the sample valves opened was characterized and it will be used to set the sample time in the valve control system; 2) steady state tare and fuel-on measured helium mole fractions matched CFD predicted values within 0.07 mole fraction, but pitot pressures were 15 to 20% lower than those predicted by CFD; 3) the CTA temperature varied by no more than $\pm 0.8^\circ\text{F}$ (from the 68°F set point), which, based on the sensitivity to temperature shown in Figure 9(a), does not introduce significant error in deduced helium mole fraction; 4) the CTA pressure was lower than the 0.5 psia set point and was not maintained constant (steady state values were between 0.3 and 0.4 psia); this was later determined to be caused by the vacuum regulator not performing well under low/no flow conditions and 5) the positions of the bow shocks off the test bed plate leading edge and the fuel plume, as seen in the schlieren, matched CFD predictions, however, visualization around the gas sampling probes was not clear enough to determine if the shocks were swallowed.

A modification to the Demo system was made to resolve the pressure regulator issue, and has been verified to be successful in bench testing. Bench testing also revealed an undesired pressure drop between the CTA and the constant pressure reservoir. The pressure drop increases with flow rate and therefore, will also prevent the CTA pressure from remaining constant during a test, as the probes will capture a range of mass flow rates throughout the mixing region. The pressure drop is thought to be due to excessive flow restriction (as opposed to excessive line length). Modifications are being made to eliminate this pressure drop and also to determine the cause of the low pitot pressures. A second wind-tunnel test is planned using the modified Demo system.

FLOW VISUALIZATION

The nitric-oxide planar laser induced fluorescence (NO PLIF) technique will be used to visualize the fuel plume. Nitric oxide is present in low concentrations in the facility air as a result of the electric-arc

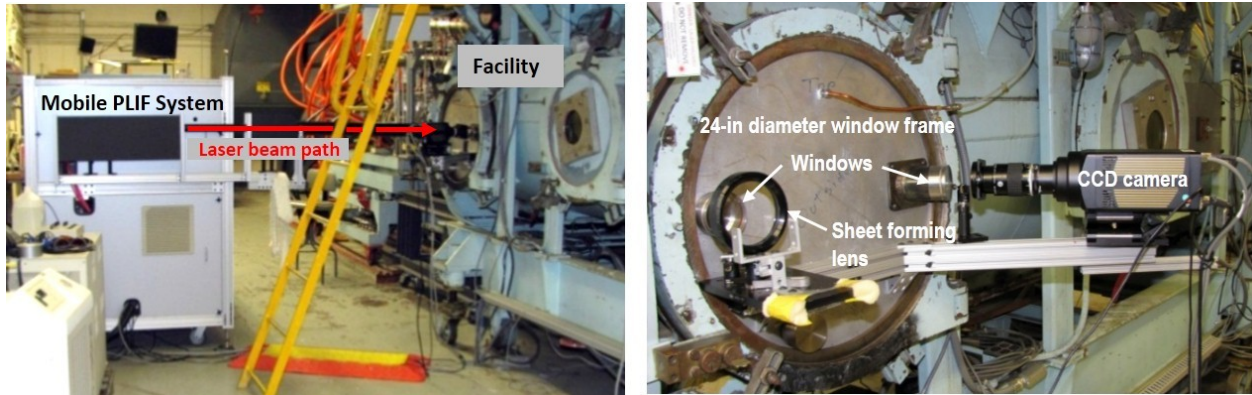


Figure 10: Photographs of the NO PLIF system set up adjacent to the AHSTF showing the mobile PLIF cart and facility (left) and detail of camera setup (right).

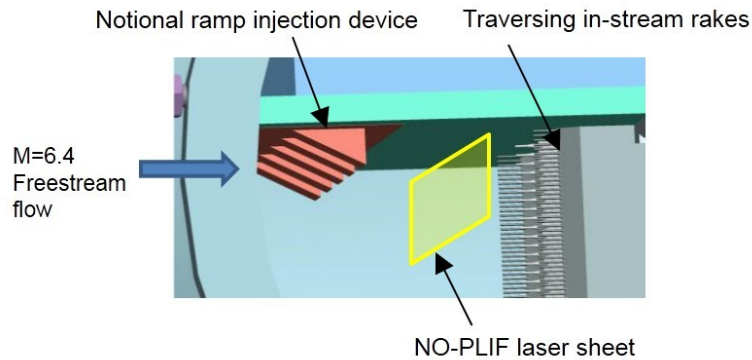


Figure 11: Notional NO PLIF survey plane for mixing tests.

heating process. This NO will act as in situ flow tracer that can be imaged using PLIF. NO PLIF uses an ultraviolet (UV) laser sheet to illuminate a planar slice in the flow containing NO. This UV light excites fluorescence from the NO molecules, which is detected by a digital camera. This PLIF technique has been employed in numerous supersonic fuel-air mixing studies.^{15–23} The present application follows closely the method of Fox et al.¹⁹ where NO is in the air stream and not the fuel (helium) stream, thus, the fuel plume is visualized by the absence of fluorescence.

One of NASA's two mobile PLIF systems capable of NO and OH PLIF imaging (details of which can be found in Johansen et al.²⁴ and Kidd et al.²⁵) has been installed next to the AHSTF test cabin as shown in Figure 10. The UV laser beam passes through optical windows mounted within the existing 24-in. diameter facility viewing window frames. The laser beam is formed into a laser sheet that passes through the fuel-air mixing region in a plane perpendicular to the main free-stream flow direction, as indicated in Figure 11. The fuel plume visualization complements the direct measurement of the helium mole fraction distribution from the GSAS and, because it provides immediate visualization, is expected to aid in the rapid screening of injection concepts.

Although levels of NO ranging from 1 to 3 mole percent are known to exist in the AHSTF test gas at typical Mach 6 to 8 flight enthalpies,^{26,27} it was unclear whether the concentration of NO at the reduced enthalpy conditions of the mixing tests would be sufficient for visualization. Furthermore, a certain level of spatial uniformity of NO must exist for the images to be interpreted properly (the lack of fluorescence interpreted as the presence of fuel). To address these concerns, a series of tests were conducted with

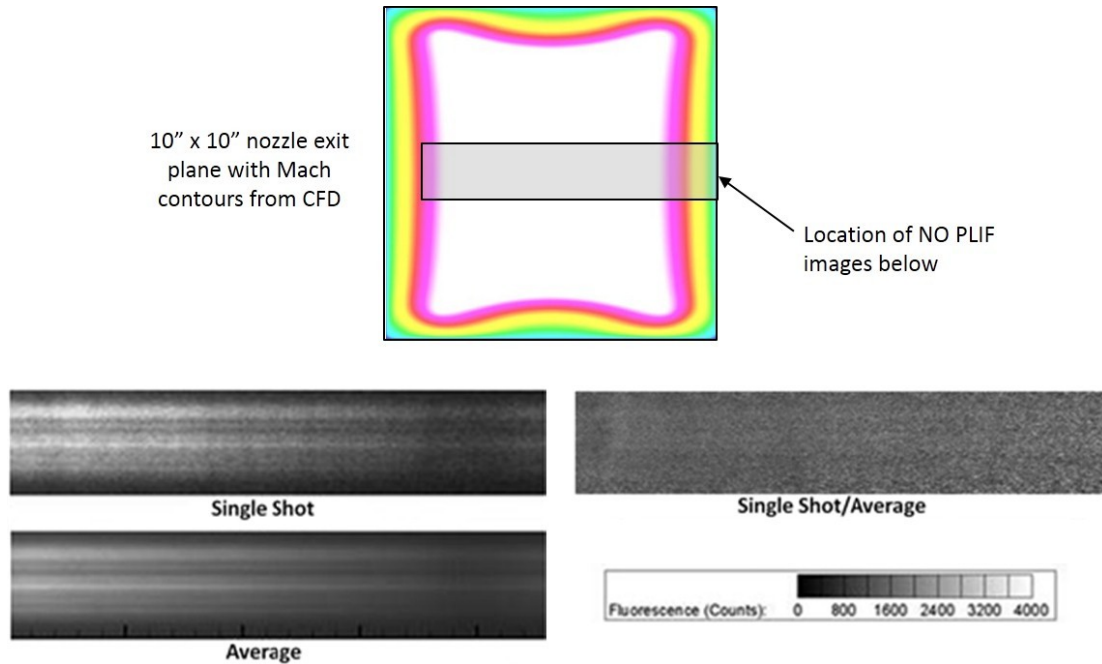


Figure 12: Image showing location of NO PLIF images (top) and sample single-shot and averaged images (left) and a single-shot imaged divided by the average (right).²⁵

the laser sheet positioned downstream of the nozzle exit plane.²⁵ These tests confirmed both a sufficient level and uniformity of NO exists in the nozzle-exit flow. Typical single-shot and averaged NO PLIF images are shown at the bottom (left) of Figure 12. Some nonuniformities are observed in the images. For example, horizontal stripes exist in both images. These horizontal stripes originate from unintended spatial variations in the laser sheet and are not indicative of flow nonuniformities. The gradual decrease in intensity from left to right in the images is caused by absorption of the laser sheet, which attenuates the laser sheet, thereby decreasing the signal intensity. This effect is also an artifact of the experiment and is not indicative of flow nonuniformity. Both of these effects can be corrected in image processing, yielding a more uniform flowfield from which fuel-air mixing can be discerned. For example, as shown in Figure 12, a single shot image can be divided by an averaged image to remove the striations and left-to-right signal variations from absorption. Such processing suggests that the actual nonuniformity of NO in the flow is about 10% of the mean level of NO.²⁵ This level of nonuniformity is deemed small enough to study fuel-air mixing, which has a nearly infinite dynamic range of fuel concentrations (some regions will contain pure fuel while others will have zero fuel).

COMPUTATIONAL ANALYSIS

CFD analysis plays an essential and integral role in the present mixing project. Increased understanding of the flow physics that control mixing requires details of the flowfield (such as the strength and location of shock/expansion waves, vortices and shear layers) that are unobtainable from the experimental data alone. Furthermore, although the experimental data can be used to characterize the fuel plume by parameters such as maximum fuel mass fraction decay and plume area growth, CFD will be needed to quantify performance metrics (such as mixing efficiency, total pressure loss and stream thrust potential). Therefore, the experimental data will be used to identify potentially high mixing performance schemes, but the CFD (calibrated and validated using the experimental data) will be used for the final performance assessment. Additionally, pretest CFD simulations provide valuable information to aid the

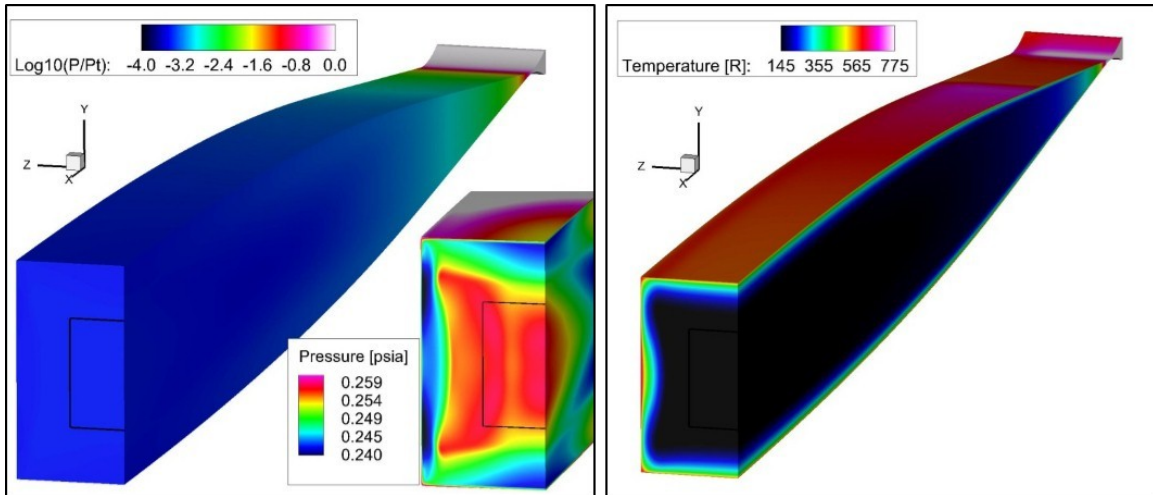


Figure 13: Pressure and temperature contours from CFD simulation of facility nozzle at the min-temperature test condition.

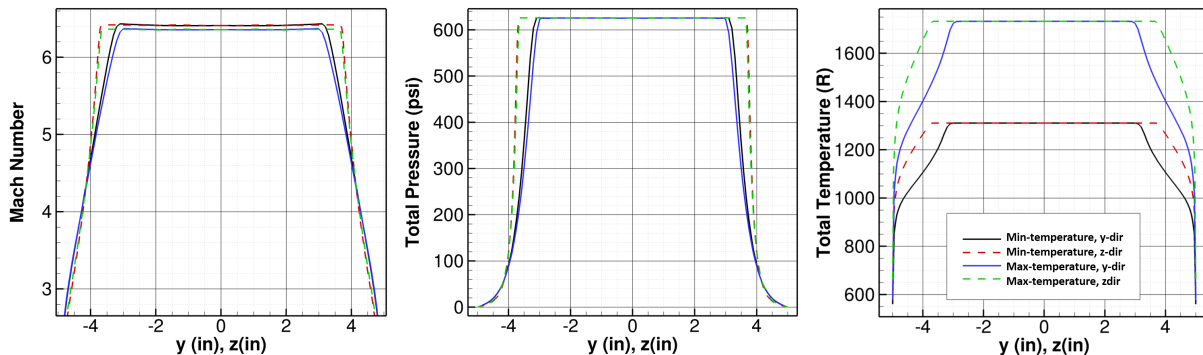


Figure 14: Mach number, total pressure and total temperature profiles from CFD simulations of facility nozzle at the min-temperature and max-temperature test conditions.

experimental design. Details of the pretest simulations and results are reported elsewhere,²⁸ but results that specifically aided design of the experimental apparatus and measurement systems are highlighted here. All simulations were performed with the VULCAN CFD code.⁵

NOZZLE SIMULATIONS

Three-dimensional Reynolds-averaged simulations (RAS) of the Mach 6 nozzle flow at the planned test conditions (Table 1) were performed to ascertain the exit flow uniformity and core size for these off-design conditions for the nozzle and to provide inflow conditions for simulations of the mixing flow-field. Example results are shown in Figure 13, which shows static pressure and static temperature contours for the min-temperature test condition. Thermodynamic calculations²⁹ at the predicted exit static pressure and temperature (0.26 psia and 145°R) confirm that the air will be in a gaseous state. Nozzle exit Mach number, total pressure and total temperature profiles for both the min-temperature and max-temperature conditions are shown in Figure 14. Examination of these profiles shows the size

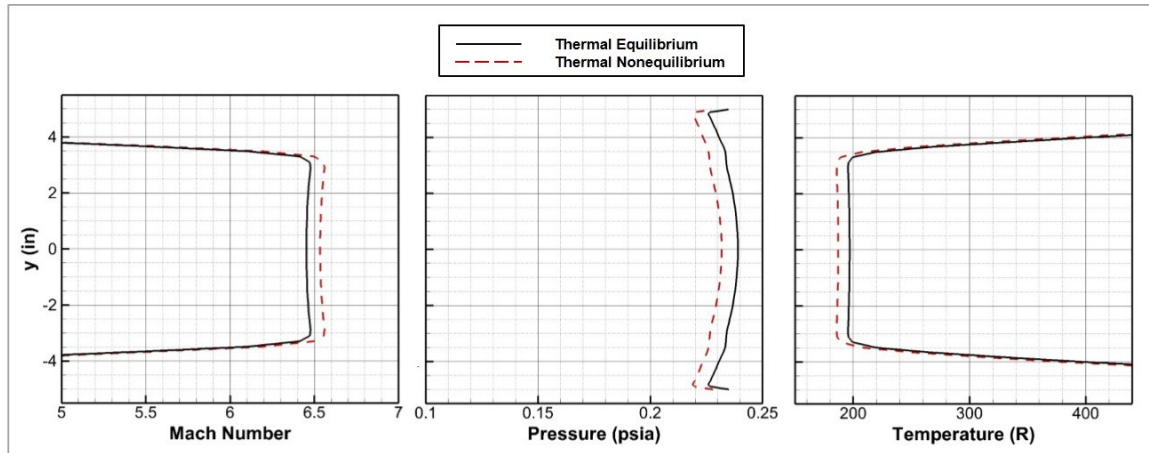


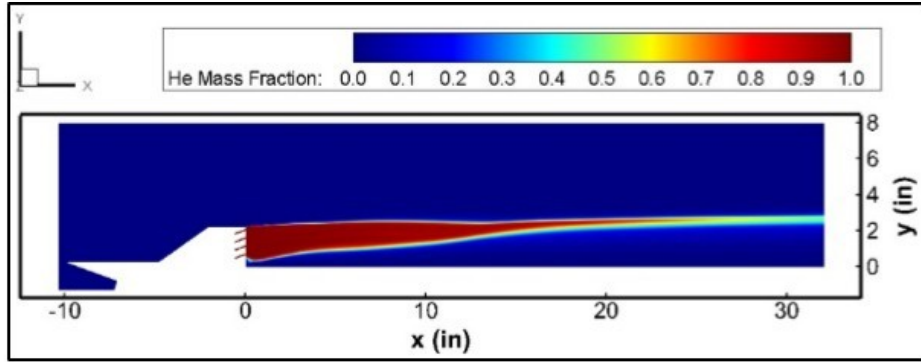
Figure 15: Effects of vibrational non-equilibrium on the nozzle exit flow properties at the max-temperature test condition.

of the uniform core region to be 6 inches high (y-direction) by 7 inches wide (z-direction). This core size guided the conservative choice of a 5-in. x 5-in. in-stream measurement plane and limits the scale of injection devices to be tested. The effects of vibrational non-equilibrium were also investigated with two-dimensional simulations of the nozzle flow at the max-temperature test condition (1760°R) and were found to be very small: the maximum effect was a 5% decrease in static temperature, as shown in Figure 15. Taken all together, these results indicate that for further analyses, the inflow to the mixing region may be simplified by assuming it to be gaseous, uniform and in thermal equilibrium.

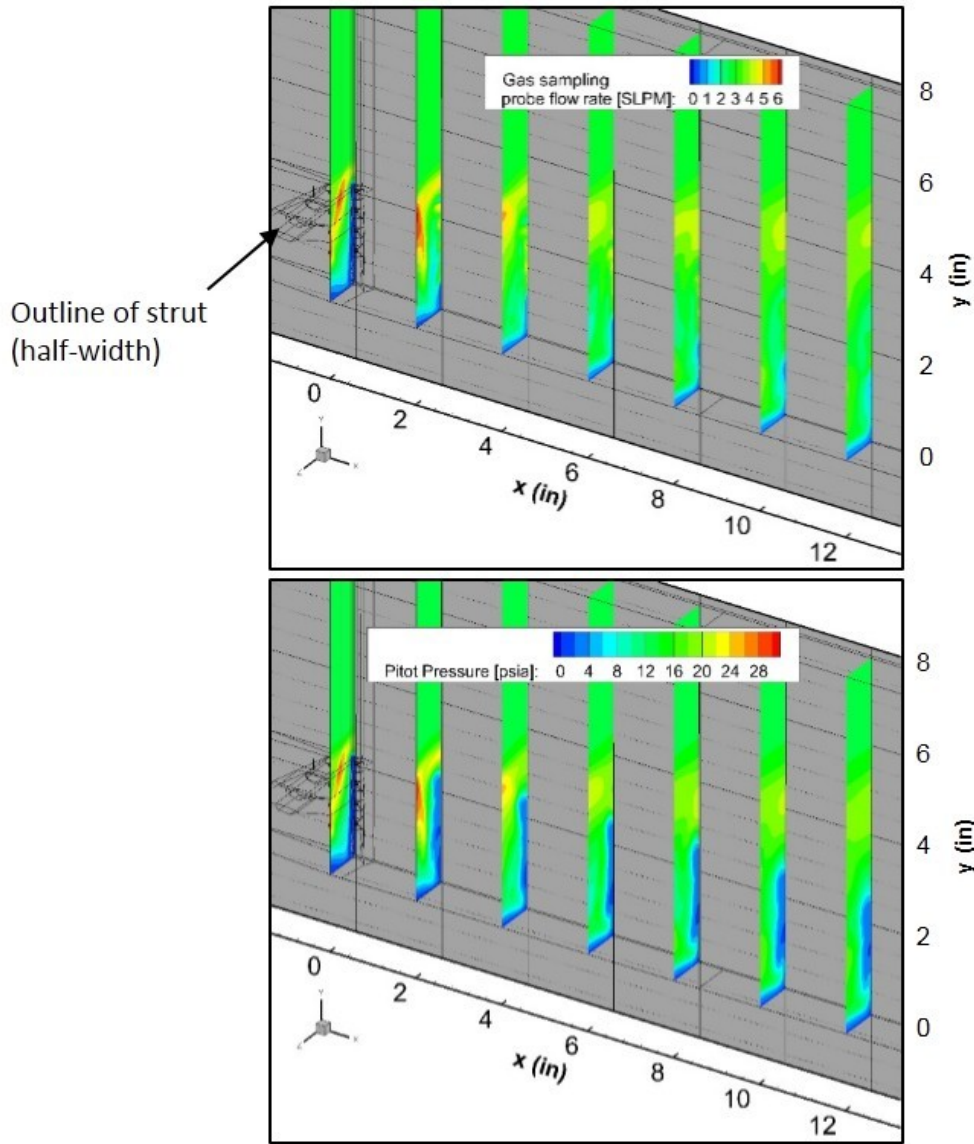
MIXING SIMULATIONS

Simulations of the flow along the test bed plate with helium injection from the baseline strut injector were performed to provide pretest predictions of the conditions in the mixing flowfield. Results of the simulation at the min-temperature test condition with helium injection at an equivalence ratio of 1.0 are shown in Figure 16. Figure 16(a) shows helium mass fraction contours in a vertical plane of the flowfield passing through the center of the strut ($z=0$) and is shown to orient the reader to the overall flowfield. Note the test bed plate and injector are inverted relative to the orientation shown in Figure 2 and $x=0$ corresponds to the base of the strut. This simulation provided the needed in-stream conditions for the design of the GSAS as described below. Additionally, although not described here, results of CFD simulations of the mixing flowfield were used to confirm the heat transfer coefficient and the recovery temperature used in the thermal-structural analysis of the test bed plate.

The key parameters in the design of the GSAS were the probe flow rate, because it sizes the system components (tubing, valves, pumps) and the freestream pitot pressure, because, along with flow rate, it drives the transfer tube back pressure (which is equal to the CTA pressure). At every point in the CFD solution, the pitot pressure was calculated as well as the flow rate through a shock-swallowed probe, given the capture area of the probe tip. Resulting contours of the pitot pressure and probe flow rate are shown at several axial planes downstream of the injector in Figure 16(b). (The regions of higher than freestream pitot pressure and mass flow are due to the shocks off the strut). The system components were designed assuming the maximum predicted probe flow rate of 6 SLPM. For the probe shock to be swallowed at every point in the flow, the transfer tube back pressure must be less than the freestream pitot pressure by an amount at least equal to the pressure drop in the transfer tube, which is a function of the probe flow rate. Analysis of the flow through the transfer tube, given the freestream pitot pressures and probe flow rates, showed that a back pressure of 0.5 psia would satisfy this requirement for



(a)



(b)

Figure 16: CFD simulation results for the mixing flowfield with a single baseline injector.

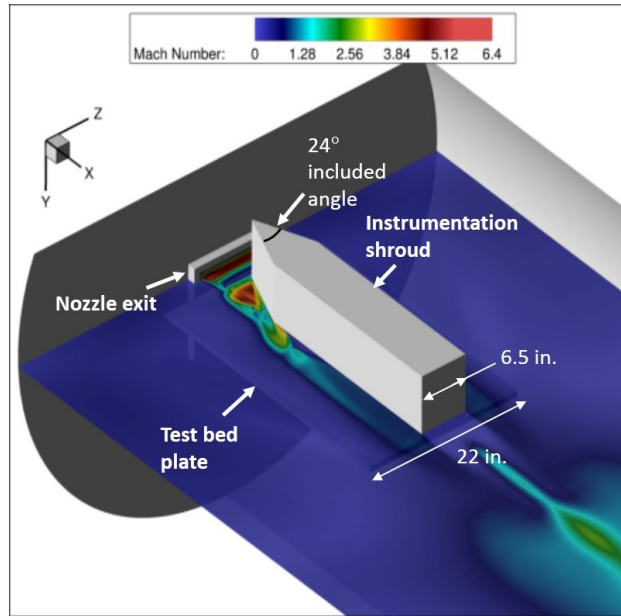


Figure 17: Isometric view of geometry included in test cabin simulations, with Mach contours above the plate shown for the 0.15 psia back pressure case.

most of the flowfield, the exceptions being the regions of low pitot pressure very near the wall and in the center of the fuel plume where the helium mass fraction is near 1.0. Inability to obtain measurements in these locations was deemed acceptable.

TEST CABIN SIMULATIONS

To investigate the interaction of the facility nozzle flow with the test cabin and the mixing test apparatus, simulations were performed of the test bed plate and shroud, installed in a 19-ft. section of the 4-ft. diameter test cabin, just downstream of the nozzle exit. Jet stretchers were not included. Helium was injected from an array of flush wall injectors on the test bed plate. These simulations were conducted at both the minimum and maximum expected test cabin back pressures of 0.15 and 2.0 psia (as expected at the beginning and end of the originally planned 5 minute test, respectively) and thus, bound the range of expected expansion/shock wave structures emanating from nozzle exit. As described below, these test cabin simulations were useful in confirming that the width of test bed plate and the lengths of the jet stretchers were adequate.

The test bed plate had been conceptually designed to be 12 inches wide, just exceeding the width of the facility nozzle. But there was concern that the flow over the top of the test bed plate, diverted by the shroud, would spill to the bottom of the plate and interfere with the flow in the mixing region. Simulations were then performed for a 22-in. wide plate around a 6.5-in. wide shroud. Figure 17 shows an isometric view of the test apparatus as viewed from above, as a visual aid to show the geometric features and flowfield over the top of plate. The facility nozzle and portions of the test cabin walls are shown. The leading edge of the test bed plate is 2.5 inches below the top of the facility nozzle. The most prominent feature is the instrumentation shroud but the test bed plate is visible just below a horizontal plane showing Mach number contours from the CFD solution for the 0.15 psia back pressure case. Close examination of the velocity vectors on the side edges of the plate for both the 0.15 psia and 2.0 psia back pressure cases showed that there was no spillage from the top of the plate to the bottom. Ultimately, a wider shroud (10.5 inches) was needed to accommodate instrumentation and fuel lines and the plate

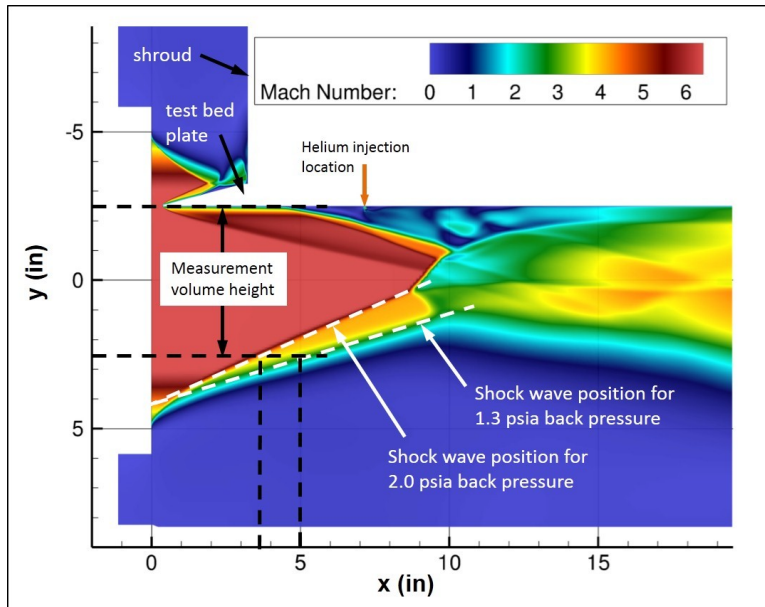


Figure 18: Mach contours in a vertical plane passing through the center of the facility nozzle and test cabin for the 2.0 psia back pressure case.

width was increased to 32 inches. Although CFD was not performed for this configuration, this width is judged to be sufficient based on the results for the 22-in. plate because it provides an additional 3 inches of lateral distance between the shroud and the side edges of the plate.

The test cabin simulations also helped to finalize the length of the jet stretchers. Inviscid shock calculations were initially used to determine that a 5-in. x 5-in. in-stream measurement plane must lie within 5.6 inches of a jet stretcher exit plane in order to remain inside a “clean” flow volume, unaffected by the shock waves. Thus, four sets of jet stretchers were designed in 5-in. incremental lengths to cover the desired 20-in. long portion of the measurement volume downstream of the injectors. Figure 18 shows Mach number contours in a vertical plane passing through the centerline of the nozzle and test bed plate for the 2.0 psia back-pressure case. The nozzle exit plane is at $x=0$. The leading edge of the test bed plate is positioned 2.5 inches below the top of the nozzle to center the measurement volume in the nozzle core flow. By overlaying a projection of the boundary of the 5-in. high measurement volume, it can be seen that the measurement plane must lie no more than 3.5 inches downstream of a jet stretcher exit plane to stay inside a clean flow volume. The earlier calculation used for the jet stretcher design had predicted the same shock angle (24°) but neglected the nozzle boundary layer, which, at a thickness of 1.5 inches, significantly offsets the position of the shocks and reduces the length of the clean flow region. However, because the test duration was subsequently limited to 3.5 minutes, the maximum test cabin pressure is expected to be only 1.3 psia. The lower shock wave angle corresponding to this back pressure was calculated and the wave is shown overlaid on Figure 18, but now accounting for the boundary layer. This shows that a 5-in. long region of clean flow will exist and that the designed jet stretcher lengths are adequate. Furthermore, the maximum back pressure was calculated assuming no evacuation of the test cabin during a test, but in fact, continuous evacuation will be active, so that the maximum back pressure will be somewhat lower than 1.3 psia.

SUMMARY

A research project aimed at enhanced injection and mixing for scramjet engines is underway at the NASA Langley Research Center. The project is a combined experimental and computational research effort to study the fundamental physics of injection and mixing relevant to scramjets at flight Mach numbers greater than 8, with an ultimate goal of improving scramjet performance and design capability. The experiments are to be conducted in the NASA Langley Arc-Heated Scramjet Test Facility under Mach 6 cold flow conditions using helium as the fuel simulant. Measurements include in-stream helium mole fraction, pitot pressures and total temperatures. Nitric oxide planar laser-induced fluorescence (NO PLIF) imaging is to be used for visualization of the fuel plume. The experiments will be used for exploring injection concepts, evaluating fuel plume characteristics (maximum fuel mass fraction decay and plume area growth) and for calibrating CFD simulations. CFD is used to obtain the details of the flowfield unobtainable from the experiments and to calculate the mixing performance metrics (mixing efficiency, total pressure recovery and stream thrust potential).

Progress made toward the project thus far includes hardware fabrication, risk reduction testing and pretest numerical simulations of the experiment. A majority of the test hardware has been fabricated including the test bed plate, jet stretchers, the in-stream rakes and traverse system and both the full scale and a smaller demonstration version of the gas sampling and analysis system (GSAS). Various demonstration tests have been conducted to reduce risk. These include facility long duration tests, which revealed that the maximum test duration was 3.5 minutes; demonstration of the NO PLIF technique at the facility nozzle exit, which showed that a sufficient quantity and uniformity of NO exists in the facility air for flow visualization; and wind-tunnel tests of the demonstration GSAS using a two probe rake, which uncovered issues related to maintaining constant CTA pressure. Finally, pretest numerical simulations of the experimental flowfields provided valuable information that aided many aspects of the experimental design. These include simulations of the facility nozzle flow, which 1) predicted the size of the core flow at the nozzle exit and therefore guided the physical scale of the mixing experiment and 2) showed the effects of vibrational non-equilibrium to be negligible; simulations of the mixing region that provided the freestream conditions needed to design the GSAS and for thermal analysis of the test bed plate; and simulations of the flow in the test cabin around the test apparatus, which ensured that the test bed plate width and jet stretcher lengths were adequate to prevent flow spillage from the top of the plate and shock waves from the nozzle exit, respectively, from interfering with the flow in the mixing region.

FUTURE WORK

Near term plans include a second test entry with the Demo GSAS to verify the modifications made to the system to maintain constant CTA pressure. The second entry will also include schlieren visualization with improved focus around the gas sampling probes as well as a demonstration of the NO PLIF technique in the mixing flowfield. The second Demo GSAS test will be followed by integration and verification testing of the of the full GSAS, the rake traverse system and their integrated control systems. Final mechanical design and fabrication of the baseline 5-strut injector block will be completed. Uncertainties in the experimental measurements will be quantified. Until experimental data is available from the mixing tests, the pretest CFD will continue to be used in several ways. It serves not only as starting point for detailed study of the mechanisms that control mixing, but also is being used to develop data post-processing and analysis tools.

REFERENCES

- [1] Heiser, W. H. and Pratt, D. T., *Hypersonic Airbreathing Propulsion*, AIAA (1994).

- [2] Guy, R. W., Torrence, M. G., Sabol, A. P., and Mueller, J. N., **Operating Characteristics of the Langley Mach 7 Scramjet Test Facility**, Tech. Rep. TM-81929, NASA (1981).
- [3] Thomas, S. and Guy, R., **Expanded Operational Capabilities of the Langley Mach 7 Scramjet Test Facility**, Tech. Rep. TP-2186, NASA (1983).
- [4] Guy, R. W., Rogers, R. C., Puster, R. L., Rock, K. E., and Diskin, G. S., **The NASA Langley Scramjet Test Complex**, in *32nd AIAA, ASME, SAE and ASEE Joint Propulsion Conference*, AIAA-96-3243, Lake Buena Vista, FL (Jul. 1996).
- [5] <http://vulcan-cfd.larc.nasa.gov> (2016).
- [6] Gruber, M. R., Nejad, A. S., and Dutton, J. C., **Circular and Elliptical Transverse Injection into a Supersonic Crossflow – The Role of Large-Scale Structures**, in *AIAA 26th Fluid Dynamics Conference*, AIAA-95-2150, San Diego, CA (Jun. 1995).
- [7] Gaffney, R. and Korte, J., **Analysis and Design of Rectangular-Cross-Section Nozzles for Scramjet Engine Testing**, in *42nd AIAA Aerospace Sciences Meeting and Exhibit*, AIAA-2004-1137, Reno, NV (Jan. 2004).
- [8] Baurle, R. A., Fuller, R. P., White, J. A., Chen, T. H., Gruber, M. R., and Nejad, A. S., **An Investigation of Advanced Fuel Injection Schemes for Scramjet Combustion**, in *36th Aerospace Sciences Meeting and Exhibit*, AIAA-1998-937, Reno, NV (Jan. 1998).
- [9] Winovich, W., **On the Equilibrium Sonic-Flow Method for Evaluating Electric-Arc Air-Heater Performance**, Tech. Rep. TN D-2132, NASA (1964).
- [10] Waitz, I., **An Investigation of Contoured Wall Injectors for Hypervelocity Mixing Augmentation**, Ph.D. thesis, California Institute of Technology (1991).
- [11] Ninneman, T. A. and Ng, W. F., **A Concentration Probe for the Study of Mixing in Supersonic Shear Flows**, *Experiments in Fluids*, 13:98–104 (1992).
- [12] Cutler, A. D. and Johnson, C. H., **Analysis of Intermittency and Probe Data in a Supersonic Flow With Injection**, *Experiments in Fluids*, 23:38–48 (1997).
- [13] Doerner, S. E. and Cutler, A. D., **Effects of Jet Swirl on Mixing of a Light Gas Jet in a Supersonic Airstream**, Tech. Rep. CR-1999-209842, NASA (Dec. 1999).
- [14] Reis, V. H. and Fenn, J. B., **Separation of Gas Mixtures in Supersonic Jets**, *Journal of Chemical Physics*, 39(12):3240–3250 (1963).
- [15] Hartfield, R. J., Abbitt, J., and McDaniel, J. C., **Injectant Mole-Fraction Imaging in Compressible Mixing Flows Using Planar Laser-Induced Iodine Fluorescence**, *Optics letters*, 16(16):850–852 (1989).
- [16] Clemens, N. T. and Mungal, M. G., **Large-scale Structure and Entrainment in the Supersonic Mixing Layer**, *Journal of Fluid Mechanics*, 284:171–216 (1995).
- [17] Island, T. C., Urban, W. D., and Mungal, M. G., **Quantitative Scalar Measurements in Compressible Mixing Layers**, in *AIAA 34th Aerospace Sciences Meeting and Exhibit*, AIAA-96-0685, AIAA, Reno, NV (Jan. 1996).
- [18] Donohue, J. M. and McDaniel, J. C., **Computer-controlled multiparameter flowfield measurements using planar laser-induced iodine fluorescence**, *AIAA Journal*, 34(8):1604–1611 (1996).
- [19] Fox, J. S., Houwing, A. F. P., Danehy, P. M., J., G. M., Mudford, N. R., and Gai, S. L., **Mole-Fraction-Sensitive Imaging of Hypermixing Shear Layers**, *Journal of Propulsion and Power*, 17(2):284–292 (2001).

- [20] Gaston, M. J., Houwing, A. F. P., Mudford, N. R., Danehy, P. M., and Fox, J. S., ***Fluorescence Imaging of Mixing Flowfields and Comparisons with Computational Fluid Dynamic Simulations***, *Shock Waves*, 12(2):99–110 (2002).
- [21] Rossmann, T., Mungal, M. G., and Hanson, R. K., ***Nitric-Oxide Planar Laser-Induced Fluorescence Applied to Low-Pressure Hypersonic Flow Fields for the Imaging of Mixture Fraction***, *Applied Optics*, 42(33):6682–6695 (Nov. 2003).
- [22] Rossmann, T., Mungal, M., and Hanson, R. K., ***Mixing Efficiency Measurements Using a Modified Cold Chemistry Technique***, *Experiments in Fluids*, 37(4):566–576 (Aug. 2004).
- [23] Takahashi, H., Ikegami, S., Oso, H., Masuya, G., and Hirota, M., ***Quantitative Imaging of Injectant Mole Fraction and Density in a Supersonic Mixing***, *AIAA J.*, 46(11):2935–2943 (2008).
- [24] Johansen, C., Danehy, P. M., Ashcraft, S. W., Bathel, B. F., Inman, J. A., and Jones, S. B., ***Planar Laser-Induced Fluorescence of Mars Science Laboratory Reaction Control System Jets***, *Journal of Spacecraft and Rockets*, 50(4):781–792 (2013).
- [25] Kidd, F. G., Narayanaswamy, V., Danehy, P. M., Inman, J. A., Bathel, B. F., Cabell, K. F., Hass, N. E., Capriotti, D. P., Drozda, T. G., and Johansen, C. T., ***Characterization of the NASA Langley Arc-Heated Scramjet Test Facility Using NO PLIF***, in *30th AIAA Aerodynamic Measurement Technology and Ground testing Conference*, AIAA-2014-2652, AIAA, Atlanta, GA (Jun. 2014).
- [26] Howard, R. P., Dietz, K. L., McGregor, W. K., and Limbaugh, C. C., ***Nonintrusive Nitric Oxide Density Measurements in the NASA Langley Arc-Heated Scramjet Test Facility***, Tech. Rep. TR-90-29, Arnold Engineering and Development Center (1991).
- [27] Cabell, K. F. and Rock, K. E., ***A Finite Rate Chemical Analysis of Nitric Oxide Flow Contamination Effects on Scramjet Performance***, Tech. Rep. TP-212159, NASA (2003).
- [28] Drozda, T. G., Axdahl, E. L., and Cabell, K. F., ***Pre-Test CFD for Risk Mitigation in the Design and Execution of the Enhanced Injection and Mixing Project at NASA Langley Research Center***, in *JANNAF 46th CS / 34th APS / 34th EPSS / 28th PSHS Joint Subcommittee Meeting*, Albuquerque, NM (Dec. 2014).
- [29] Lemmon, E. W., Huber, M. L., and McLindon, M. O., ***NIST Standard Reference Database 23: Reference Fluid Thermodynamic and Transport Properties- REFPROP, Version 8.0, National Institute of Standards and Technology, Standard Reference Data Program, Gaithersburg, MD.*** (2007).